Supplementary Information:

Low loss Plasmon-assisted electro-optic modulator

Christian Haffner[1], Daniel Chelladurai[1], Yuriy Fedoryshyn[1], Arne Josten[1], Benedikt Baeuerle[1], Wolfgang Heni[1], Tatsuhiko Watanabe[1], Tong Cui[1], Bojun Cheng[1], Soham Saha[3], Delwin L. Elder[2], Larry. R. Dalton[2], Alexandra Boltasseva[3], Vladimir Shalaev[3], Nathaniel Kinsey[4], and Juerg Leuthold[1]

[1]ETH Zurich, Institute of Electromagnetic Fields (IEF), 8092 Zurich, Switzerland

[2]University of Washington, Department of Chemistry, Seattle, WA 98195-1700, USA

[3]Purdue University, School of Electrical & Computer Engineering and Brick Nanotechnology Center, West Lafayette, WIN 47909, USA

[4]Virginia Commonwealth University, Department of Electrical and Computer Engineering, Richmond, VA 23284, USA

Contents

I) Simulation Method, Geometry and Permittivity

In this chapter we introduce all the necessary simulation methods for this work, as well as the geometric and material parameters for the simulations. The top-view and cross-section of the simulation model are sketched in Fig. 1(a) and (b), respectively. The structure consist of a metal-insulator-metal (MIM) plasmonic ring with radius (R) and slot width (w_{PSW}) which is placed at a distance ($d_{Au\text{-}Si}$) above a silicon bus waveguide (h_{Si} and w_{Si}) buried in silicon dioxide. The metal ring is cladded and filled with a binary composition of two organic electro-optic (OEO) chromophores, namely 75%HD-BB-OH and 25%YlD125[1,2]. The electro-optic coefficient (r_{33}) of the material is estimated to be ~90 pm/V. The MIM ring acts simultaneously as a waveguide for surface plasmon polaritons (SPPs) and as a highly conductive electrode enabling high-speed operation. The height of the donut electrode is larger than the disk in order to reduce radiation losses due to bending, as discussed in a subsequent chapter. The cross-sectional SEM image in the main text is from an old generation of devices in which the thicker outer electrode was not yet implemented (the current chip featuring the higher sidewalls was not sacrificed for taking SEM images, as the old chip featuring the lower sidewalls is otherwise the same).

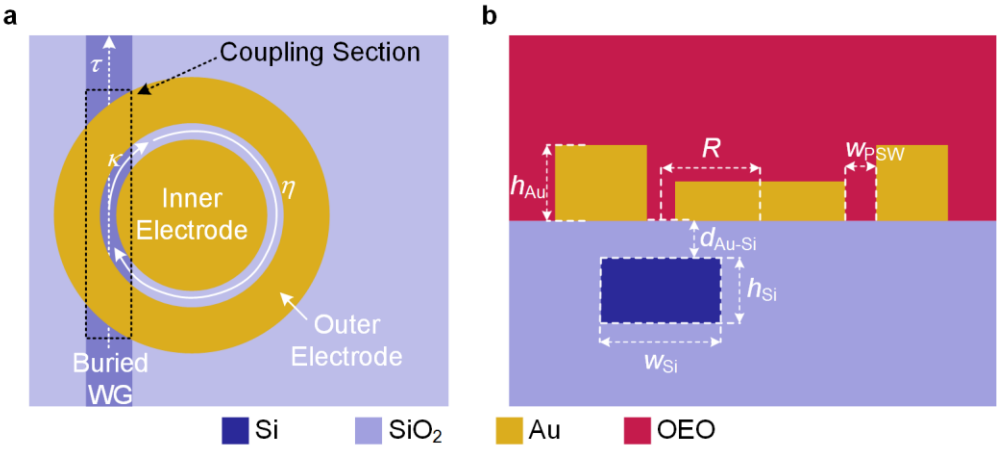

Fig. 1: Schematic representations of the plasmonic slot ring resonator. (a) Top-view showing the plasmonic ring and its alignment relative to the buried bus waveguide. The overlap of both serves as the coupling interface between the photonic and plasmonic domain. τ, κ are the field coupling parameters while η represents round trip coefficients of the field (b) Cross-section showing the buried bus waveguide with the plasmonic ring placed on top. Structural parameters are also defined..

All electromagnetic field simulations were performed with COMSOL. 2-D simulations (cylindrical coordinates) using an Eigenfrequency solver were applied to calculate the intrinsic Q-factor and the round trip coefficient, η, within a wavelength range of 1.4 μm-1.6 μm. We

calculated the coupling parameters (τ, κ and C) by 3-D simulations of the bus waveguide and half of the resonator. The coupling parameters η, τ and κ are labeled in Fig. 1(a). We used the following parameters throughout all simulations unless stated otherwise.

Table 1: Geometric Parameters of fabricated device

h_{Si}	w_{Si}	h_{OEO}	R	$h_{Au,Outer}$/ $h_{Au,Inner}$	$d_{Au\text{-}Si}$	w_{PSW}
220 nm	450 nm	800 nm	1000 nm	350 nm/ 150nm	70 nm	60-80 nm

We assumed a constant permittivity of 3.48 and 1.44 for silicon and silicon dioxide, respectively. The optical properties of HD-BB-OH/YLD124 are taken from ref. [2] to account for dispersion and losses within the material, while its RF-permittivity is assumed to be 4.5 similar to other OEO-materials[3]. The permittivity of gold was taken from our ellipsometry measurements [4], while the permittivity of silver and copper was taken from ref. [5].

II) Operating principle

In this chapter we discuss the operating principle with the help of the ring's transfer function, Fig. 2(a), and the simulated electric field distribution, Fig. 2(b) – (e). The upper row shows the simulated field in the off-resonance case, while the lower row represents the on-resonance case. The left column and right column depict the field in the bus waveguide and the field in the ring resonator planes, respectively.

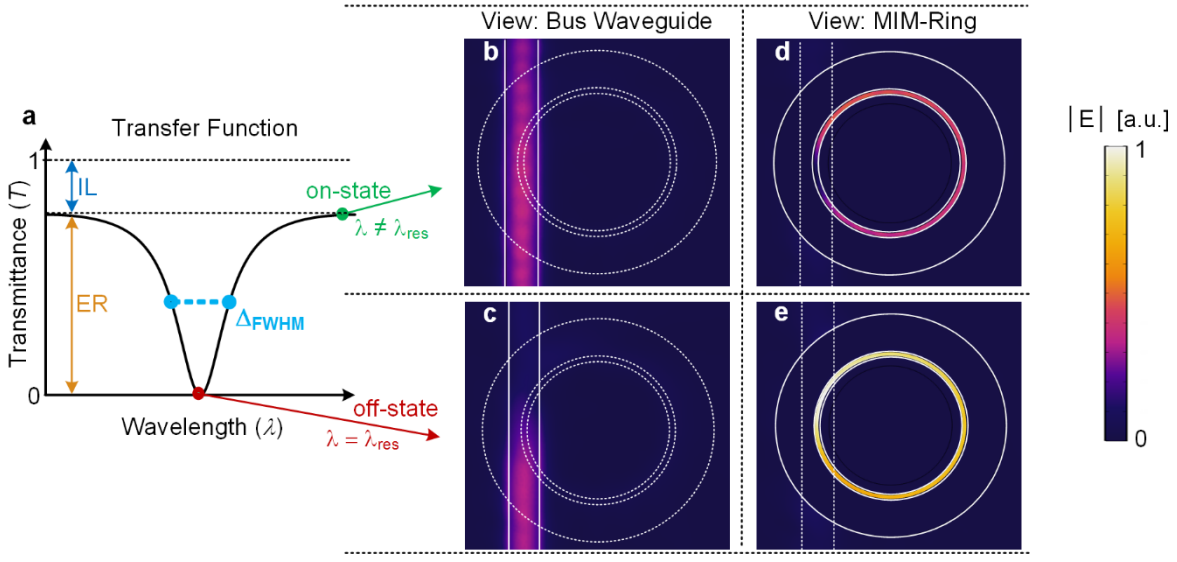

Fig. 2: Transfer function and simulated mode profiles representations of the plasmonic slot ring resonator. (a) Transmittance versus wavelength (λ) of a notch-filter with its characteristic properties: insertion loss (IL), extinction

ratio (ER), full-width at half maximum (Δ_{FWHM}). The Q-factor is given by the ratio of $\lambda_{res}/\Delta_{FWHM}$ larger Q built a stronger interference within the ring which results in a much sharper notch-filter. (b) to (e) simulated field profiles of the device presented in Fig 1(c) of the main manuscript. The left column shows the field in the plane of the bus waveguide, while the right one shows the norm of the electrical field in the plane of the ring resonator. The field intensity within the ring is larger than in the bus waveguide due to the plasmonic (sub-λ confinement) and resonant enhancement (multiple roundtrips). The top row, (b) and (d), represents the field distribution in the on-state (off-resonance) when the field interferes destructively within the ring as shown by the zero field intensity in the ring in coupling section. The bottom row, (c) and (e),shows the off-state (on-resonance).

Light travelling through the bus waveguide reaches the coupling section where there is a modal overlap between the bus waveguide and the plasmonic slot waveguide (PSW) of the ring. This results in a fraction of the light, given by $|\kappa|^2$, Fig. 1(a), coupling into surface plasmon polaritons (SPPs) in the ring as is known from directional couplers[6]. The remaining fraction of light, $|\tau|^2$, continues through the bus waveguide. In the "on" state, the SPP finishes one round-trip and interferes destructively with itself as indicated by the electrical field being zero in the PSW above the bus waveguide, see Fig. 2(d). This leads to nearly-full transmission through the bus waveguide after accounting for reflections and ohmic losses in the coupling section, see Fig. 2(b). The "off" state is the result of SPPs meeting the ring's resonance condition and constructively interfering within the ring, see Fig. 2(e). This leads to destructive interference in the bus waveguide and an extinction in transmission, see Fig. 2(c).

The transmission through the bus waveguide is dependent on the resonance condition of the plasmonic ring

$$\lambda_{\mathrm{res,m}} = \frac{2\pi R \cdot (n_{\mathrm{SPP}} + \Delta n_{\mathrm{SPP}})}{m}, \tag{1}$$

$\lambda_{\mathrm{res,m}}$ is the resonance wavelength of the m$^{\mathrm{th}}$ azimuthal mode. n_{SPP} is the effective refractive index and Δn_{SPP} indicates that resonance wavelength can be shifted by tuning the effective refractive index of the SPP. This enables a wide field of applications such as electro-optic (EO) modulation or sensing.

III) Analytical Framework of a Plasmonic Notch Filter

In this section, we summarize the analytical framework to describe the transmission through a bus waveguide coupled to a ring resonator, based on the work of Yariv et al. [7]. Using this framework, we develop an algorithm serving as a fast toolbox for a rough optimization and qualitative discussion of the resonators properties. Such a framework is required because modes

in sub-µm, bent MIM waveguides cannot be easily computed with commercial tools, unlike the case for µm-sized, bent photonic waveguides. The steady state power transfer function (T) of a single bus waveguide coupled to a ring or disc resonator (notch-pass filter) can be derived as

$$T = \frac{\eta^2 C^2 + |\tau|^2 - 2\eta C|\tau|\cos(\beta_{\mathrm{SPP}} l)}{1 + \eta^2|\tau|^2 - 2\eta|\tau|\cos(\beta_{\mathrm{SPP}} l)} \tag{2}$$

Here, β_{SPP} is the propagation constant of SPPs within the resonator. l is the circumference of the resonator. η is the round trip coefficient of the SPPs, whereas η^2 defines the power attenuation of the SPPs after one round trip. τ is the transmission coefficient through the bus waveguide. κ is the coupling coefficient between the mode of the bus waveguide and the mode of the plasmonic resonator. C describes the efficiency of the coupling section and is given by the sum of the transmission and coupling efficiencies (i.e. $|\kappa|^2 + |\tau|^2 = C \leq 1$). These parameters are highlighted in Fig. 1(a). C is only equal to unity in the lossless case. In reality, the non-zero length and plasmonic character of the coupling section means a fraction of the propagating wave is lost due to reflections and/or heat dissipation[8]. C mainly affects the achievable IL, as shown in Fig. 3 as a function of the propagation loss in the ring (i.e. $L_{\mathrm{SPP}} = 1 - \eta^2$).

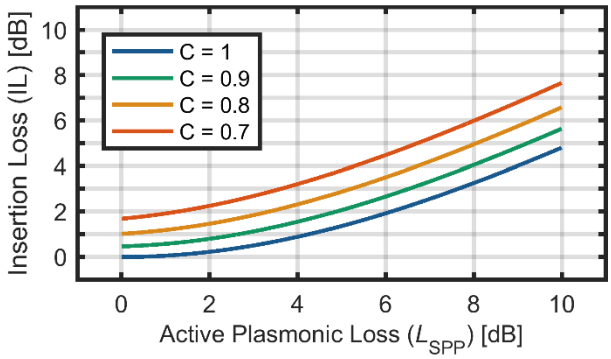

Fig. 3: Total IL over the loss in the active plasmonic section (L_{SPP}) for various coupling efficiencies (C). The bypassing mechanism enables lower IL than light would experience when completely traveling through the plasmonic section (e.g. IL < L_{SPP}).

In the ideal case of critical coupling ($\eta C = \tau$) the transmission drops to zero at the resonance frequency (ω_{res}) as the light is pulled into the resonator. The light, which constructively interferes within the ring, simultaneously destructively interferes with the light in the bus waveguide. Losses in resonators ($L_{\mathrm{SPP}} = 1 - \eta^2$) are normally described by the quality factor (Q), which can easily be extracted from simulation and experiments. Therefore, we derive an approximate expression for the round trip attenuation coefficient (η) as a function of the unloaded Q factor. We

distinguish between the quality factors of a stand-alone resonator and a resonator coupled to a bus waveguide as unloaded (Q_{unloaded}) and loaded (Q_{loaded}), respectively.

We start with the definition[7]

$$\eta = e^{-\delta t_{RT}}, \tag{3}$$

where δ is the attenuation coefficient of the field over time and t_{RT} is the round trip time of a SPP in the ring. We first take the common approximation of the unloaded Q-factor

$$Q_{\mathrm{unloaded}} \approx \frac{\omega_{\mathrm{res}}}{2\delta}, \tag{4}$$

where ω_{res} is the resonance frequency and δ is again the attenuation coefficient of the field over time. This approximation is valid for large Q-factors but leads to an underestimation of Q for small values.

Next, t_{RT} corresponds to the round trip time of a SPP in the ring and is dependent on the SPP's group refractive index (n_{g}), the ring's radius, R, and the speed of light in vacuum, c_0:

$$t_{\mathrm{RT}} = \frac{2\pi R}{c_0} n_{\mathrm{g}} = \frac{2\pi R}{c_0}\left(n_{\mathrm{eff}} - \lambda_0 \cdot \frac{dn_{\mathrm{eff}}}{d\lambda}\right). \tag{5}$$

We approximate $n_{\mathrm{g}} \approx$ by n_{eff}. (The resulting error is ~10-15% with larger error for smaller slot widths and shorter wavelengths due to plasmonic dispersion[2]). The effective refractive index is related to the resonance frequency ω_{res} and azimuthal mode number (m) by

$$n_{\mathrm{eff}} = \frac{2\pi c_0}{\omega_{\mathrm{res}}} \frac{m}{2\pi R}. \tag{6}$$

Thus, we can rewrite our original equation for the round trip coefficient as a function of the azimuthal mode number and the unloaded Q-factor

$$\eta = e^{-\pi \frac{m}{Q_{\mathrm{unloaded}}}}. \tag{7}$$

Details on simulation can be found in Chapter 0. Fig. 4(a) and Fig. 4(b) show the simulated Q-factor and η, respectively. Each quantity is presented in the form of a heat map as functions of the resonator's radius (R) and plasmonic slot width (w_{PSW}).

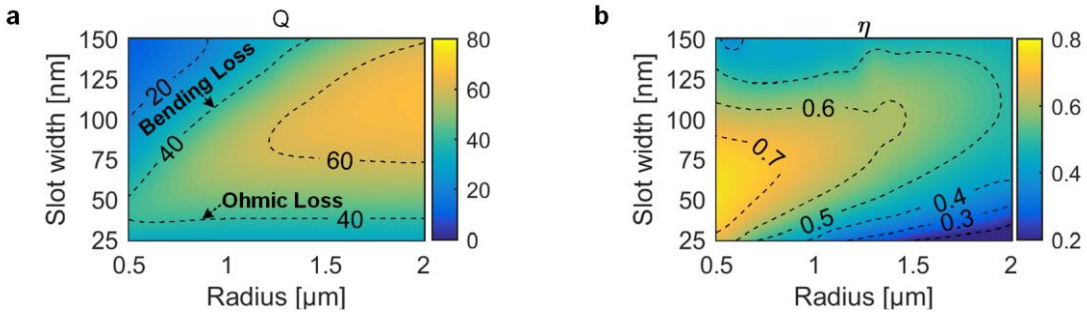

Fig. 4: Characteristic properties of the plasmonic ring resonator. **(**a) Unloaded *Q*-factor versus radius and slot width. The contour lines follow a triangular shape as different loss mechanism dominate (bending versus slot width), see section IV). (b) Round trip coefficient $\boldsymbol{\eta}$ as functions of the plasmonic slot waveguide width (w_{PSW}) and the resonator's radius (*R*). Optimal operation in terms of *IL* is achieved for small radius as η increases. The optimal slot width depends on the trade-off between ohmic loss (narrower slots) and bending loss (wider slots).

We observe the following:

- There exists an optimal slot width for each radius. Increasing the slot width from the optimum results in larger bending loss while decreasing the slot width leads to increasing plasmonic/ohmic losses.
- The Q-factor decreases towards smaller radii due to increasing bending losses. Larger slot widths are more susceptible to this trend since the mode is less confined.
- For η, the optimum slot width decreases as the radius decreases. The maximum η is observed at the smallest radius. This suggests that the benefit of higher unloaded Q-factors at larger radii is not enough to compensate for the higher losses incurred from the extra oscillation cycles.

In total η between 0.5 up to 0.7 can be achieved with Q-factors ranging from 70 down to 40, respectively. From this, we obtain with help of equation (2) IL of ~1.5 dB for $\eta^2 = 0.7^2 = -3$ dB when assuming a conservative value for the coupling section efficiency ($C \approx 0.8$). Furthermore, such low insertion losses are achievable while simultaneously achieving an infinite theoretical extinction ratio due to critical coupling. Section (V) discuses in more detail how to achieve this critical coupling.

IV) Q-Factor Loss Contributions

For a better understanding of the last three points regarding Fig. 4, we consider the actual loss mechanisms that contribute to the unloaded Q-factor and how each is affected by the radius and slot width. The total loss in the resonator is composed of two parts: bending losses due to radiation in a bent waveguide and propagation losses due to material absorption and sidewall scattering.

Each are represented by their own attenuation coefficient, δ, and combine linearly to give a total attenuation, $\delta_{total} = \delta_{bend} + \delta_{prop}$. Since the Q-factor can be determined as $Q = {\omega_{\mathrm{res}}}/{2\delta}$ we can consider each source of loss to have its own Q-factor, which combine to give the total Q-factor as:

$$\frac{1}{Q_{\mathrm{total}}} = \frac{1}{Q_{\mathrm{bending\,loss}}} + \frac{1}{Q_{\mathrm{propagation\,loss}}} \tag{8}$$

Propagation loss in a PSW is dependent on the width of the slot[4]. The loss increases towards smaller slot widths, since the stronger confinement pushes more of the field into the metal where ohmic losses occur. This singular dependence results in the flat trend line in Fig. 4(a) at small slot widths where propagation loss dominates.

Bending loss occurs due to radiation leakage from a bent waveguide and is larger for smaller bends. It is also dependent on how strongly the mode is confined. Stronger confinement in smaller slots leads to smaller bending losses for a given bend radius. The dependence on radius and slot width results in the diagonal trend line in Fig. 4(a) at small radii and large slot widths where bending loss dominates.

Both types of losses can be reduced with proper selection of materials and geometry. Propagation loss can be improved simply by choosing metals with smaller plasmonic losses like silver or the CMOS-compatible copper. Bending losses can be improved for instance by using a larger height for the outer electrode (h_{Au} in Fig. 2). The effect is shown in Fig. 5, where the Q-factors corresponding to bending loss are given for an outer electrode height of (a) 350 nm and (b) 150 nm. $Q_{\mathrm{bending\,loss}}$ is simulated by assuming a loss-less metal. To understand why the larger outer-wall height is beneficial, one can use the analogy of a barrier preventing leakage out of the ring. The higher the barrier, the more the leakage is inhibited.

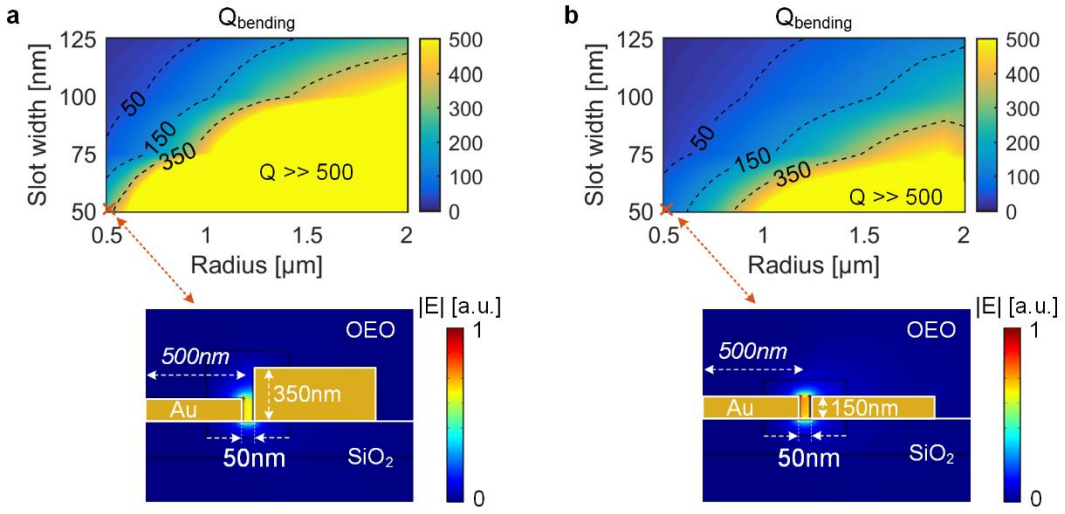

Fig. 5: Bending loss contribution of a ring resonator with an outer electrode height of (a) 350 nm and (b) 150 nm. Bending losses increase with larger slot width and narrower radius, as the plasmonic character of the mode becomes less pronounced.

V) Critical Coupling

Critical coupling (ER → ∞) requires a specific amount of energy to be coupled from the bus waveguide to the PSW, as determined by $\eta C = \tau$. Photonic resonators have low round trip losses, and thus, require a weakly coupled system of bus waveguide and resonators. In contrast, the lower Q-factors of plasmonic resonators requires a strongly coupled bus waveguide to guarantee enough energy exchange for building up constructive and destructive interference (bypassing mechanism). Here, we show that already our simple implementation is sufficient to achieve sufficient ER with low IL.

The coupling and transmission coefficient of our system can be well-controlled by changing the gap distance ($d_{\text{Au-Si}}$) between the bus waveguide and a plasmonic slot waveguide and their interaction length [6]. Fig. 6 shows each of $|\tau|^2$, $|\kappa|^2$, and C as function of the ring radius (interaction length) and gap distance (coupling strength) . The closer the distance, the greater the coupling (i.e. κ) and vice versa. The opposite holds true for τ. The radius also affects each parameter because a larger radius extends the coupling section. It therefore increases the coupled fraction, decreases the transmitted fraction and decreases the coupling section efficiency (due to the larger ohmic loss and scattering loss),

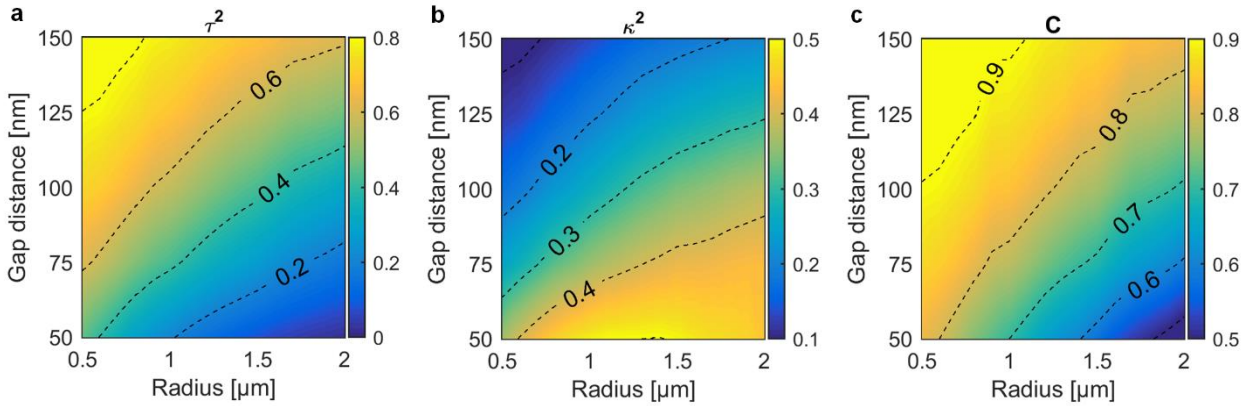

Fig. 6: Coupling parameter dependencies on the resonator's radius and the distance between the resonator and bus waveguide. (a) Transmitted fraction, (b) Coupled fraction, and (c) Coupling section efficiency for a resonator with a plasmonic slot width of 60 nm.

From Fig. 6,we estimate that our fabricated device (gap ~75 nm, radius 1 μm) has a coupling efficiency of 0.8 and couples approximately 40% to the ring, while transmitting the other 40%.

Fig. 7(a) shows the critical coupling (CC) condition ($\eta C - \tau$). Under-coupling ($\eta C < \tau$) and over-coupling ($\eta C > \tau$) of the resonator changes its properties. For instance, under coupling results in lower IL, larger Q-factors but reduced ER while over-coupling diminishes performance of all three. Therefore, resonators should be operated at CC if large ERs are required or under-coupled when small IL are desired. Fig. 7(b) and (c) show the achievable IL and ER for a slot width of 60 nm and various combinations of ring radius and gap distance, respectively. The dashed lines mark the 10 dB ER and the 3 dB IL levels. Insertion losses below 3 dB can be achieved for a large parameter space.

Please note, that the ER drops for 2 μm and a gap distance of 50 nm even though CC is fulfilled. This is due to a lack of interpolation points in this area.

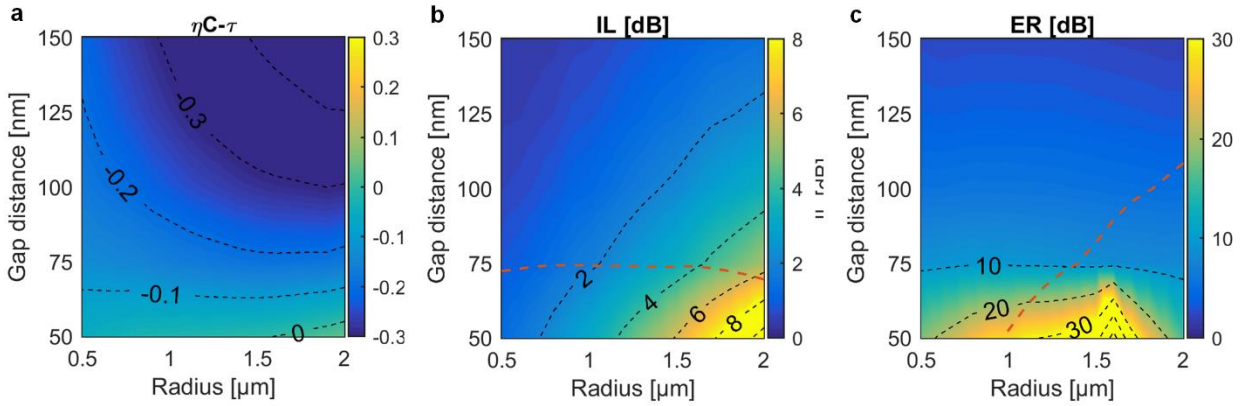

Fig. 7: Critical coupling condition, ER and IL as a function of radius and gap distance for a slot width of 60nm. (a) critical coupling condition ($\boldsymbol{\eta C = \tau}$) shows that for a large parameter space the ring resonator is under-coupled.

However, comparing IL (b) and ER (c) shows that despite under-coupling ER are above 10 dB with IL below 3 dB are achievable. The dashed lines marking in (b) a 10 dB ER and in (c) a 3 dB IL.

The coupling is defined by the spacing between bus waveguide and resonator. Our simulations show that fabrication variations of ±25nm result in strong performance fluctuations see Fig. 7. Controlling the spacing ($d_{Au,Si}$), and thus the critical coupling, can be reliably achieved by a vertical layer stack. In contrast, if the plasmonic resonator and bus waveguide are in the same horizontal layer, the critical coupling condition is difficult to achieve due to the limited resolution of a lithography's alignment system (i.e. 10s of nm).

VI) Comparison of 3D-Simulation and Experimental Results

Fig. 8 shows the simulated and measured field profiles of the two ring resonators with radiii (a) R = 1030 nm and (b) R = 1080 nm, that were presented in Fig. 1(c) of the main manuscript. In general, the measurements match the simulations well with a few minor differences.

- The ILs are below 2.7 dB and show 1 dB excess ILs in experiments compared to simulations, which we attribute to the fabrication imperfections. For instance, the Au lift-off process results in non-vertical sidewalls, which in theory increases the bending losses (IL↑; Q↓).
- ERs are >10 dB and 2 dB smaller in experiments compared to simulations as the increased bending losses result in less coupling relative to the critical coupling condition, see section V).
- We attribute the difference of 12.5 nm in the resonant wavelength, Fig. 8(b), to uncertainties when extracting the device geometry from SEM images.

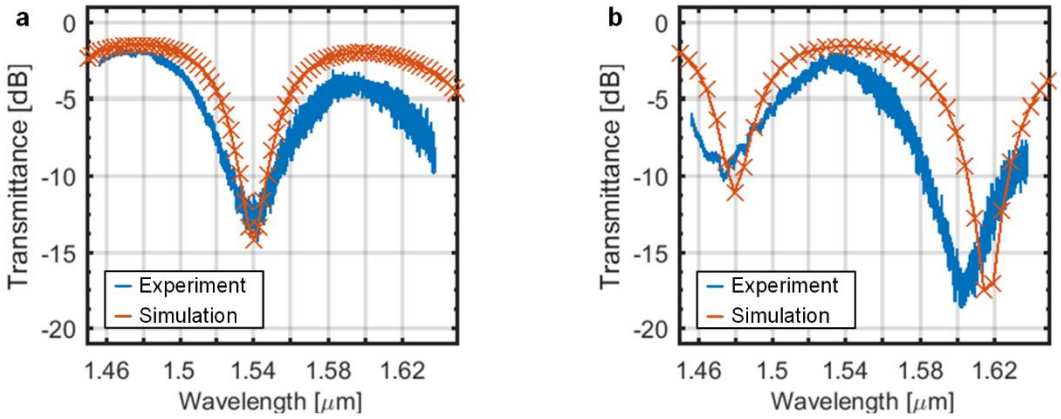

Fig. 8: Comparison of 3D and 2D Simulations. (a) *R* of 1080 nm and (b) *R* of 1030 nm. The geometrical parameters for the simulation where extracted by means of SEM images. The measured slot width was 60 nm rather than the designed 80 nm. All other parameters matched well with the given values in Table 1.

Table 2 Comparison of key characteristics between simulation and experimental results - * interpolated values

	Device (a)		Device (b)	
Characteristics	Sim.	Exp.	Sim.	Exp.
IL_{1550nm} [dB]	1.6*	2.7*	1.4	2.5
ER_{1550nm} [dB]	12.5	10	10.5*	8.8*
Q	~40	~30	37	~29
FSR [nm]	118	122	140	130
Finesse	~3.1	~2.4	3.8	2.6
λ_{res} [nm]	1540	1540	1487.5	1475

VII) Resonant Enhancement

We analytically compare the phase sensitivity of a plasmonic ring resonator's power transfer function (*T*)

$$T_{\mathrm{R}} = \frac{\eta^2 C^2 + |\tau|^2 - 2\eta C|\tau|\cos(\Delta\varphi)}{1 + \eta^2|\tau|^2 - 2\eta|\tau|\cos(\Delta\varphi)}, \tag{9}$$

and a plasmonic Mach-Zehnder's (MZ) power transfer function [9]

$$T_{\mathrm{MZ}} = \frac{C^2\eta^2}{2}(1 + \cos(2\Delta\varphi)). \tag{10}$$

The latter comprises two plasmonic slot waveguides embedded within a MZ-interferometer and is operated in a push-pull configuration enabling a phase shift twice as large as compared to a one-armed MZ. Both devices uses the change of the SPPs' effective refractive index to induce a

phase shift ($\Delta\varphi = \Delta n_{\mathrm{SPP}} \cdot l$) that translates into a change of the output power (ΔT). The sensitivity is $S_{T(\varphi)} = \delta T/\delta\varphi$ and for a critically coupled ring resonator

$$\frac{\delta T_{\mathrm{R}}}{\delta\varphi} = \frac{2C^2\eta^2 \cdot (C\eta^2 - 1)^2 \cdot \sin(\Delta\varphi)}{(C^2\eta^4 - 2C\eta^2 \cdot \cos(\Delta\varphi) + 1)^2}, \tag{11}$$

while in the case of a MZ

$$\frac{\delta T_{\mathrm{MZ}}}{\delta\varphi} = -C^2\eta^2 \cdot \sin(2 \cdot \Delta\varphi). \tag{12}$$

The ratio between both derivatives defines the resonant enhancement (*RE*) when comparing a ring resonator with a push-pull MZ interferometer. In the following discussion, both devices feature the same lengths/circumference ($l = 6\ \mu\mathrm{m}$), plasmonic losses ($L_{\mathrm{SPP}} = 1 - \eta^2 = 3.7\ \mathrm{dB}$), photonic to plasmonic coupling efficiencies ($C = 0.8$) and φ. Please note, these values correspond to the estimated parameters of the fabricated resonators.

Fig. 9 shows both transfer functions and the absolute value of their first derivatives as functions of the phase.

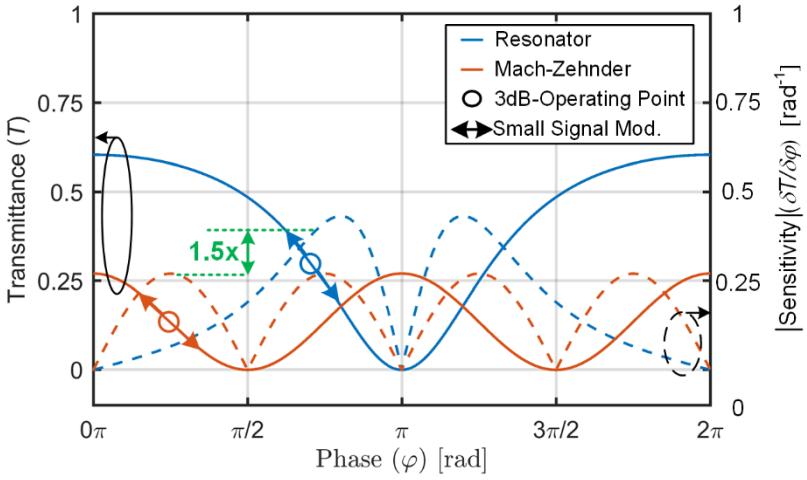

Fig. 9: Calculated transmittance and absolute sensitivity over the wavelength of a ring resonator (blue) and push-pull Mach-Zehnder interferometer. The sensitivity of the resonator is 1.5 times larger, enabling shorter devices, and thus, reducing the overall losses of plasmonic modulators.

The notch filter response of the ring resonators results in a higher slope of T compared to the MZ and the resonant enhancement (*RE*) is 1.5 when both are operated in their 3dB-point. This results in different changes of the transmission

$$\Delta T = \frac{\delta T}{\delta\varphi} \cdot \Delta\varphi \propto \frac{\delta T}{\delta\varphi} \cdot \Delta n_{\mathrm{SPP}} \cdot l. \tag{13}$$

Therefore, a MZ needs to be 1.5 times longer than the ring resonator's circumference, which results in larger losses in the plasmonic section. For simplicity, we neglected that $\frac{\delta S_{T(\varphi)}}{\delta \eta} \neq 0$. Furthermore, we use the -3dB point of the transmittance as the operating point as this results in lower IL compared to operation at maximal sensitivity of a resonator.

Please note, that the push-pull configuration can be easily implemented with EO-effects as oppositely biased slot waveguides push the phase in one arm while pulling it in the other. In contrast, most sensor materials are not capable of such operation and MZ sensors require one arm to be a passive slot waveguide. In this case, the *RE* is two times larger.

Fig. 10(a) shows the sensitivity of both configurations as a function of the active plasmonic losses L_{SPP}. The *RE* increases exponentially for low losses. The vertical dashed lines serves as references and indicate the typical losses of our ring resonators.

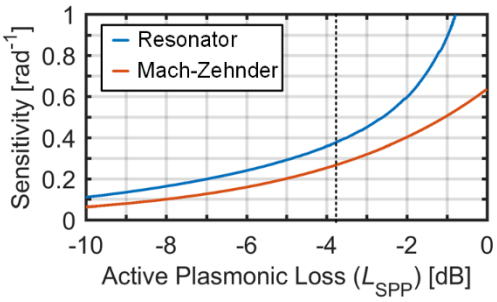

Fig. 10: Sensitivity of a ring resonator and MZ-modulator. The x-axes indicate the losses in the active plasmonic section. The *RE* enhancement starts to kick in at low losses but still provides an enhancement of the sensitivity ($S_{T(\lambda)}$) for larger L_{SPP} due to the lower overall insertion loss of the resonator.

VIII) References

1 D. L. Elder *et al.* University of Washington", are prepering a manuscript to be called "Electro-optic chromophores with rigid aromatic bridge-protecting units". (2017).

2 Haffner, C. *et al.* Harnessing nonlinearities near material absorption resonances for reducing losses in plasmonic modulators. *Optical Materials Express* **7**, 2168-2181, doi:10.1364/OME.7.002168 (2017).

3 Hoessbacher, C. *et al.* Plasmonic modulator with 170 GHz bandwidth demonstrated at 100 GBd NRZ. *Opt. Express* **25**, 1762-1768, doi:10.1364/OE.25.001762 (2017).

4 Haffner, C. *et al.* All-plasmonic Mach–Zehnder modulator enabling optical high-speed communication at the microscale. *Nat Photon* **9**, 525-528, doi:10.1038/nphoton.2015.127

5 McPeak, K. M. *et al.* Plasmonic Films Can Easily Be Better: Rules and Recipes. *ACS Photonics* **2**, 326-333, doi:10.1021/ph5004237 (2015).

6 Delacour, C. *et al.* Efficient Directional Coupling between Silicon and Copper Plasmonic Nanoslot Waveguides: toward Metal−Oxide−Silicon Nanophotonics. *Nano Letters* **10**, 2922-2926, doi:10.1021/nl101065q (2010).

7 Yariv, A. Critical coupling and its control in optical waveguide-ring resonator systems. *IEEE Photonics Technology Letters* **14**, 483-485, doi:10.1109/68.992585 (2002).

8 Bozhevolnyi, S. I., Volkov, V. S., Devaux, E., Laluet, J.-Y. & Ebbesen, T. W. Channel plasmon subwavelength waveguide components including interferometers and ring resonators. *Nature* **440**, 508-511 (2006).

9 Heni, W. *et al.* 108 Gbit/s Plasmonic Mach-Zehnder Modulator with >70 GHz Electrical Bandwidth. *Lightwave Technology, Journal of* **PP**, 1-1, doi:10.1109/JLT.2015.2487560 (2015).